Virus Research 316 (2022) 198796

Contents lists available at ScienceDirect

Virus Research

journal homepage: www.elsevier.com/locate/virusres

Efficient recovery of attenuated canine distemper virus from cDNA

Marianne Wyss [a,1], Vaiva Gradauskaite [a,d,1], Nadine Ebert [b,c], Volker Thiel [b,c], Andreas Zurbriggen [a], Philippe Plattet [a,*]

[a] Division of Neurological Sciences, Vetsuisse Faculty, University of Bern, Switzerland
[b] Department of Infectious Diseases and Pathobiology, Vetsuisse Faculty, University of Bern, Bern, Switzerland
[c] Institute of Virology and Immunology, Mittelhäusern, Bern, Switzerland
[d] Graduate School for Cellular and Biomedical Sciences, University of Bern, Bern, Switzerland

ARTICLE INFO

Keywords:
Morbillivirus
Reverse genetics
Phosphoprotein
Large protein
V protein
Replication

ABSTRACT

To provide insights into the biology of the attenuated canine distemper virus (CDV) Onderstepoort (OP) strain (large plaque forming variant), design next-generation multivalent vaccines, or further investigate its promising potential as an oncolytic vector, we employed contemporary modifications to establish an efficient OP-CDV-based reverse genetics platform. Successful viral rescue was obtained however only upon recovery of a completely conserved charged residue (V13E) residing at the N-terminal region of the large protein (L). Although L-V13 and L-V13E did not display drastic differences in cellular localization and physical interaction with P, efficient polymerase complex (P+ L) activity was recorded only with L-V13E. Interestingly, grafting mNeonGreen to the viral N protein via a P2A ribosomal skipping sequence (OP^{neon}) and its derivative V-protein-knockout variant (OP^{neon}-V^{ko}) exhibited delayed replication kinetics in cultured cells. Collectively, we established an efficient OP-CDV-based reverse genetics system that enables the design of various strategies potentially contributing to veterinary medicine and research.

Despite efficient available vaccines, measles virus (MeV) is still responsible for more than 200.000 human deaths per year (Patel et al., 2020). Beyond vaccination purposes, which saved millions of human lives, the attenuated strain of MeV additionally exhibits promising results in the treatment of various types of cancers in humans (Cattaneo and Russell, 2017; Robinson and Galanis, 2017; Ungerechts et al., 2017) and represents an innovative platform for the development of multivalent vaccines (Bodmer et al., 2018; Frantz et al., 2018; Gerke et al., 2019; Muhlebach, 2017; Nurnberger et al., 2019). The attenuated strain of the related canine distemper virus (CDV), which is also used as a very efficient live-attenuated vaccine, was equally reported to kill cancer cells, both *in vitro* and *in vivo*, although for the latter, mice with xenografts of persistently infected canine cancer cells were used as a model system (Del Puerto et al., 2011; Garcia et al., 2017; Pfankuche et al., 2017; Suter et al., 2005). A reverse genetics platform based on an attenuated CDV strain is therefore of great interest in veterinary medicine. Indeed, such a system may not only offer the molecular basis to refine our knowledge of the biology of the attenuated CDV strain, but also to further investigate its potentials as an oncolytic vector. However, reported reverse genetics technologies based on the large plaque forming variant of the attenuated Onderstepoort (OP) strain (Gassen et al., 2000; Parks et al., 2002), which was initially obtained by serial passages in ferret and in chorio-allantoic membrane of embryonated hen's eggs, lacked modern molecular modifications allowing efficient recovery from cDNA (Beaty et al., 2017). This may result in suboptimal generation of recombinant viruses; a low recovery rate that may preclude the rescue of engineered recombinant viruses featuring impaired infectivity profiles.

MeV and CDV are enveloped infectious agents carrying single-stranded RNA genomes of negative polarity. They belong to the genus *Morbillivirus* of the family *Paramyxoviridae* (Lamb and Parks, 2007; Maes et al., 2019). Cell entry is the first step of their life-cycle and relies on a process called membrane fusion, which occurs at the plasma membrane at neutral pH (Plattet et al., 2016). The membrane fusion mechanism is controlled by the interacting surface glycoproteins (H and F) as well as a specific host cell surface receptor. The RNA genome is tightly encapsidated by N proteins and together with associated RNA-dependent RNA polymerases (RdRp; assembly of P- and L-proteins) they define a supra-molecular structure, termed ribonucleoprotein (RNP) complex.

* Corresponding author.
E-mail address: philippe.plattet@vetsuisse.unibe.ch (P. Plattet).
[1] These authors contributed equally to this work.

https://doi.org/10.1016/j.virusres.2022.198796
Received 7 March 2022; Received in revised form 21 April 2022; Accepted 4 May 2022
Available online 11 May 2022

Such RNP complexes represent the minimal unit necessary to drive both the transcription and replication steps, which exclusively occur in the cytoplasm. The matrix protein is the essential viral component that regulates the packaging and ensuing cell exit process at the plasma membrane (Lamb and Parks, 2007). Finally, the morbillivirus C and V accessory proteins (two factors encoded from the P-gene) were not only reported to inhibit interferon-mediated antiviral responses, but viral replication efficacy as well (Caignard et al., 2009; Fontana et al., 2008; Nakatsu et al., 2008; Ramachandran et al., 2008; Rothlisberger et al., 2010; Shaffer et al., 2003; Svitek et al., 2014; Tober et al., 1998). Interestingly, it was also proposed that the C-protein may additionally act as (i) an infectivity factor by promoting efficient viral particle release, and (ii) an enhancer of the viral polymerase processivity (Devaux and Cattaneo, 2004; Pfaller et al., 2015b, 2014). The latter function may limit the generation of copy-back defective particles, which are well-known to be potent inducers of type I interferon (Pfaller et al., 2015b).

Establishment of an efficient OP-CDV-based reverse genetics platform is required to design next-generation strategies that have the potential to improve animal health in the future. However, due to different passage history performed with OP-CDV in various laboratories during the past decades, genetic variations were monitored (referred in this study to as OP-CDV variants), which eventually translated into viruses inducing either large or small syncytia (von Messling et al., 2001). Noteworthy, 5 amino acid differences were detected between two reported "large plaque forming" variants (GenBank accession numbers AF305419.1 and NC_001921.1; Table 1). We engineered an antigenomic cDNA clone based on the deposited OP-CDV sequence: AF305419.1 (Fig. 1A). This viral sequence was selected because (i) it was employed as the basis for one of the first established morbillivirus-based reverse genetics systems, and (ii) most importantly, the derived recombinant viruses were demonstrated to be non-pathogenic in ferrets (Silin et al., 2007).

Hence, consistent with the strategy used to assemble a cDNA clone of respiratory syncytial virus (Hotard et al., 2012), the antigenomic cDNA of OP was synthesized in six fragments (Eurofins Genomics) and subsequently cloned into a pBluescript-derived plasmid ($OP^{colorless}$; Fig. 1A) (Plattet et al., 2004). To enable swift viral gene engineering, restriction sites flanking each open reading frame (ORF) were designed. Note that one additional nucleotide was modified in the H-gene to destroy an RsrII restriction site without affecting the ORF (Fig. 1B and Table 3). Since the previous rescue system lacked contemporary modifications to increase viral rescue (making recovery of viruses inefficient (Gassen et al., 2000)), several key modifications, recently shown to increase rescue events, were additionally engineered (Beaty et al., 2017). We appended an optimal T7 polymerase promotor sequence (T7p-opt) followed by a hammerhead ribozyme sequence (HHrbz) to the leader region of OP, as well as the classical T7 terminator sequence (T7t) and the hepatitis delta virus ribozyme sequence (HDVrbz) to the trailer region (Fig. 1B).

Engineering of additional transcription units (ATU) into viral genetic backbone is a technology widely used in the field to produce heterologous proteins from recombinant viral genomes (de Vries et al., 2017; Duprex et al., 1999; Frantz et al., 2018; Muhlebach, 2017; Ungerechts et al., 2017). Although efficient and extremely useful for a panel of biological applications, the position of the ATU with regard to the 3′ end region of the genome has been shown to potentially influence virological features, including viral-mediated pathogenicity (Park et al., 2016; von Messling et al., 2004; Yun et al., 2015). To investigate the impact of an alternative approach, we employed the P2A "ribosomal skipping" strategy to express the brightest green fluorescent reporter protein available (mNeonGreen [neon]; Allele Biotech) from the recombinant virus (OP^{neon}; Fig. 1C). Neon was thus attached to the N ORF via the P2A sequence and, to achieve optimal efficacy, three amino acids (GSG) were added before the P2A peptide [29].

Paramyxovirus-based rescue systems require expression of the nucleocapsid (N)-, phospho (P)- and large (L)-proteins concomitantly to the delivery of genomic RNA molecules to initiate viral encapsidation and ensuing transcription/replication events (Pfaller et al., 2015a). Thus, the OP N, P/C^{ko} (silenced for C-protein expression to avoid any interference with replication efficacy) and L genes were cloned into the T7-driven pTM expression vector. We employed the vaccinia virus-free BsrT7 cell system (BHK cell stably expressing the T7 RNA polymerase) combined with a short heat shock (2 h at 42 °C) few hours post-transfection to rescue OP from cDNA (Buchholz et al., 1999). Two

Table 1
Summary of mutations between Bern clone and various OP-CDV variants.

Ref.	gen pos	nt	codon	ORF	aa pos	aa	gen pos	nt	codon	ORF	aa pos	aa
AF305419.1	1657	A	AAT	N	517	N	4104	A	AGC	M	225	S
NC_001921.1	1657	G	AGT	N	517	S	4104	T	TGC	M	225	C
Bern clone*	1657	A	AAT	N	517	N	4104	A	AGC	M	225	S
AF378705.1	1657	G	AGT	N	517	N	4104	A	AGC	M	225	S
AF305419.1	4724	T	NA	NA (M 3′UTR)	NA	NA	4942	G	AGG	F	3	R
NC_001921.1	4724	G	NA	NA (M 3′UTR)	NA	NA	4942	A	AAG	F	3	K
Bern clone*	4724	T	NA	NA (M 3′UTR)	NA	NA	4942	G	AGG	F	3	R
AF378705.1	4724	G	NA	NA (M 3′UTR)	NA	NA	4942	A	AAG	F	3	K
AF305419.1	5279	T	CAT	F	115	H	8536	G	TCG	H	486	S
NC_001921.1	5279	G	CAG	F	115	Q	8536	A	TCA	H	486	S
Bern clone*	5279	T	CAT	F	115	H	8536	G	TCG	H	486	S
AF378705.1	5279	G	CAG	F	115	Q	8536	A	TCA	H	486	S
AF305419.1	8563	G	CAG	H	495	Q	9067	T	GTG	L	13	V
NC_001921.1	8563	A	CAA	H	495	Q	9067	A	GAG	L	13	E
Bern clone*	8563	G	CAG	H	495	Q	9067	A	GAG	L	13	E
AF378705.1	8563	A	CAA	H	495	Q	9067	A	GAG	L	13	E
AF305419.1	13,097	T	GAT	L	1356	D	13,856	G	TCG	L	1357	S
NC_001921.1	13,097	C	GAC	L	1356	D	13,856	T	TCT	L	1357	S
Bern clone*	13,097	T	GAT	L	1356	D	13,856	G	TCG	L	1357	S
AF378705.1	13,097	C	GAC	L	1356	D	13,856	A	TCA	L	1357	S

Ref: GenBank accession number; gen pos: position of the nucleotide within the CDV genome; nt: nucleotide; ORF: open reading frame; aa pos: position of the amino acid within the protein sequence: aa: amino acid.
*cDNA clone (without reporters) constructed in this study derived from the reference sequence (AF305419.1) and harboring the L-V13E substitution as well as the mutations generating the unique restriction sites.
NA: not applicable.
color-coded in red: the sequence comparison with the OP-CDV small plaque forming variant (AF378705.1) focused on the positions differing between the large plaque forming variants (AF305419.1 and NC_001921.1).
Red boxes: amino acid differences between OP-CDV variants.

days post-transfection, BsrT7 cells were mixed with Vero cells expressing the canine SLAM receptor. Further viral amplification was performed in standard Vero cells (2-3 rounds).

Despite the modifications to the full-length cDNA clone, all our initial attempts to rescue OP^{neon} and OP^{colorless} from the cDNA clones systematically failed. Noteworthy, although faint green syncytia (in case of OP^{neon}) were reproducibly observed in Vero-cSLAM cells (upon cell mixing), we were unable to efficiently amplify the recombinant virus. To gain insights on possible defective mutation(s) in our cDNA clone, we employed next-generation sequencing (NGS) to obtain genetic sequences from our OP stocks. As motioned above, several nucleotide variations were expected since the passage history of OP-CDV in various laboratories differs. When compared to the deposited OP sequence (AF305419.1), 17 nucleotides variations were detected. While 12 did

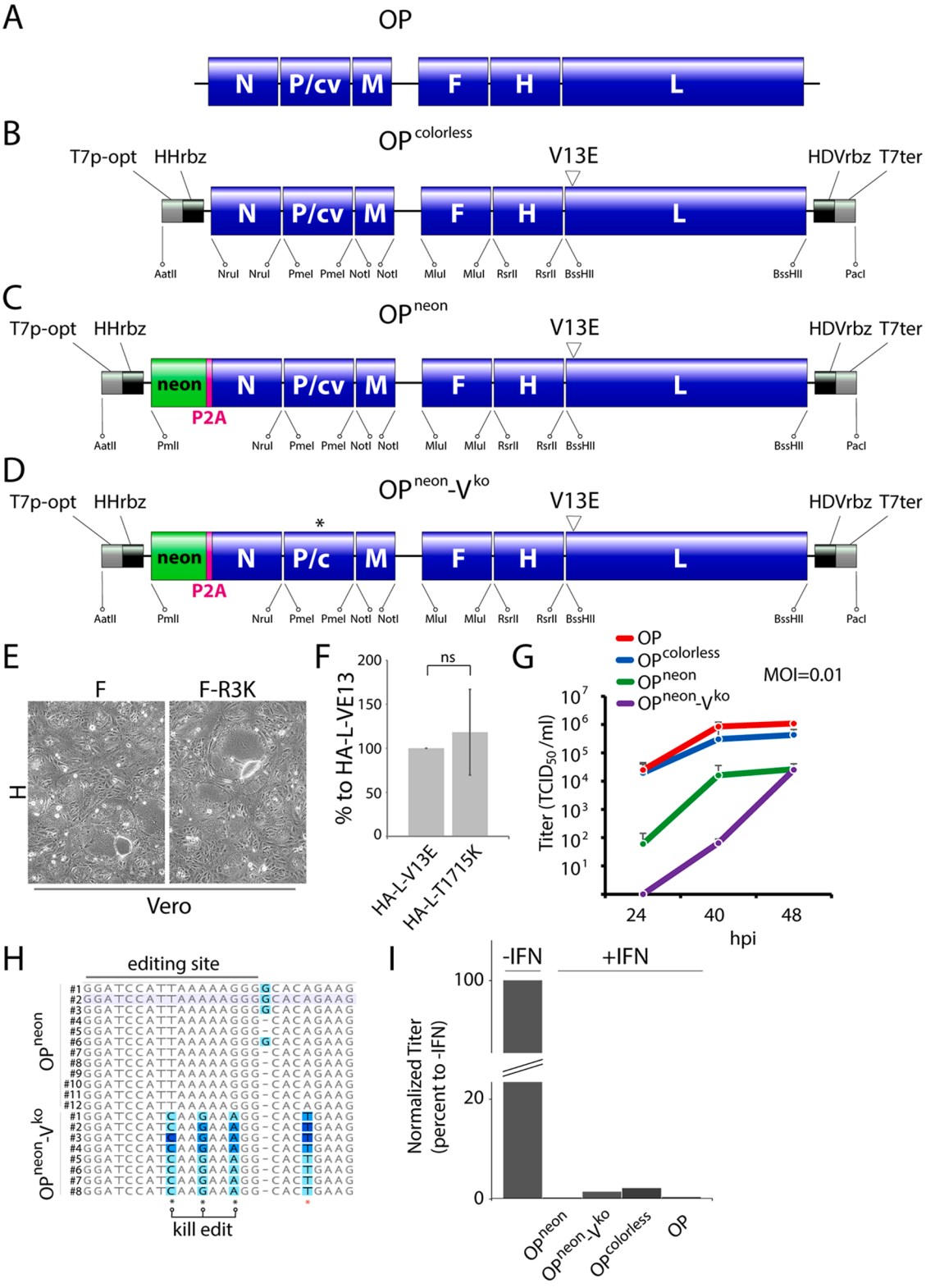

(caption on next page)

Fig. 1. Cartoon representation of CDV genomes and derived viral characterization. (A) Cartoon representation of the genome of the vaccine strain Onderstepoort (OP)-CDV (large plaque-forming variant). (B) Illustration of the assembled clone of OP-CDV ($OP^{colorless}$). (C) OP cDNA clone additionally carrying the mNeonGreen fluorescent gene (OP^{neon}). (D) OP cDNA clone carrying a mutated P-gene in order to ablate V-protein expression (OP^{neon}-V^{ko}). The asterisk indicates nucleotide substitutions that were introduced into the P-gene in order to ablate V-protein expression; "kill edit" tccattaaaaaggg into tccatcaagaaagg (mutations underlined), as well as additional mutations aiming at ablating production of the C-terminal domain of V, or potentially disrupting interactions with known cellular factors: R233stop, E235A, W246G, I247L, K249stop, C255S, and the V microdomain 288-RVWH-291 into 288-GIGD-291. Neon: mNeonGreen, T7p-opt: optimized T7 promotor sequence, HHrbz: hammerhead ribozyme sequence, HDVrbz: hepatitis D virus ribozyme sequence, T7t: T7 terminator sequence. (E) Syncytia formation in Vero cells upon co-transfection of plasmids expressing H(OP) and F(OP) or H(OP) and F(OP)-R3K. GFP was also added. Representative fields of view of fluorescence emission (monitored 24 h post transfection) are illustrated. (F) Replication complex activity of HA-L-V13E protein and derivative HA-L-T1715K variant. The graphic shows means and SD for data from three independent experiments performed in duplicates. Significance was determined using one-way ANOVA using GraphPad Prism. ns: not significant (G) Growth kinetics of $OP^{colorless}$, OP^{neon}, OP^{neon}-V^{ko} and the nonmodified parental Onderstepoort CDV vaccine strain (OP) in Vero cells. Means ± standard deviations of data from at least two independent experiments performed in duplicates are shown. MOI: multiplicity of infection, hpi: hours post infection. (H) mRNA-editing (supplementary G nucleotide insertion) is exclusively observed in OP^{neon}-infected cells. Sequence alignment of RT-PCR-amplified and cloned P-gene fragments. Black asterisks indicate the mutated positions leading to "kill edit". Red asterisk indicates the substitutions performed in the P-gene of OP^{neon}-V^{ko} to insert a stop codon (R233stop). (I) Impact of IFN treatment (1000 U/ml) on titers exhibited by OP, $OP^{colorless}$, OP^{neon} and OP^{neon}-V^{ko} (determined at 48 h in Vero cells). Means ± standard deviations of data from two independent experiments performed in duplicates are shown.

not lead to amino acid modulations, 5 did and, among them, only 3 were found to be completely fixed (F-R3K, L-V13E and L-T1715K; Table 2). Interestingly, while a lysine residue at position 3 of the F protein and 1715 of the L-protein are found in other reported OP-CDV sequences, the glutamate residue at position 13 of the L-protein is fully conserved among all investigated morbilliviruses. Thus, the valine residue found at position 13 of the L-protein is unique to the deposited OP sequence (AF305419.1) (Table 2). We nevertheless validated that the amino acid variations (F-K3 and L-K1715) were not significantly interfering with proteins' function. Indeed, no drastic difference was recorded when fusion and replication of those two protein variants were assessed in a transient cell-cell fusion assay and a minireplicon assay, respectively,

Table 2
Summary of mutations between Bern stock and various OP-CDV variants.

Ref.	gen pos	nt	codon	ORF	aa pos	aa	gen pos	nt	codon	ORF	aa pos	aa
AF305419.1	1661	T	GAT	N	518	D	2151	T	GGT	P	117	G
NC_001921.1	1661	T	GAT	N	518	D	2151	T	GGT	P	117	G
Bern stock*	1661	T/C (50%)§	GAT/C	N	518	D/D	2151	T/C (25%)§	GGT/C	P	117	G/G
AF378705.1	1661	T	GAT	N	518	D	2151	T	GGT	P	117	G
AF305419.1	2151	T	GTG	C	110	V	4458	T	NA	NA (M 3′UTR)	NA	NA
NC_001921.1	2151	T	GTG	C	110	V	4458	T	NA	NA (M 3′UTR)	NA	NA
Bern stock*	2151	T/C (25%)§	GT/CG	C	110	V/A	4458	A (100%)§	NA	NA (M 3′UTR)	NA	NA
AF378705.1	2151	T	GTG	C	110	V	4458	A	NA	NA (M 3′UTR)	NA	NA
AF305419.1	4724	T	NA	NA (M 3′UTR)	NA	NA	4942	G	AGG	F	3	R
NC_001921.1	4724	A	NA	NA (M 3′UTR)	NA	NA	4942	A	AAG	F	3	K
Bern stock*	4724	A (100%)§	NA	NA (M 3′UTR)	NA	NA	4942	A (100%)§	AAG	F	3	K
AF378705.1	4724	A	NA	NA (M 3′UTR)	NA	NA	4942	A	AAG	F	3	K
AF305419.1	6767	T	AGT	F	611	S	7005	A	NA	NA (F 3′UTR)	NA	NA
NC_001921.1	6767	T	AGT	F	611	S	7005	A	NA	NA (F 3′UTR)	NA	NA
Bern stock*	6767	C (100%)§	AGC	F	611	S	7005	C (100%)§	NA	NA (F 3′UTR)	NA	NA
AF378705.1	6767	C	AGC	F	611	S	7005	C	NA	NA (F 3′UTR)	NA	NA
AF305419.1	8536	G	TCG	H	486	S	8563	G	CAG	H	495	Q
NC_001921.1	8536	A	TCA	H	486	S	8563	A	CAA	H	495	Q
Bern stock*	8536	A (100%)§	TCA	H	486	S	8563	A (100%)§	CAA	H	495	Q
AF378705.1	8536	A	TCA	H	486	S	8563	A	CAA	H	495	Q
AF305419.1	9067	T	GTG	L	13	V	10,496	G	CCG	L	489	P
NC_001921.1	9067	A	GAG	L	13	E	10,496	G	CCG	L	489	P
Bern stock*	9067	A (100%)§	GAG	L	13	E	10,496	G/A (20%)§	CCG/A	L	489	P/P
AF378705.1	9067	A	GAG	L	13	E	10,496	A	CCA	L	489	P
AF305419.1	12,383	C	TTC	L	1118	F	13,097	T	GAT	L	1356	D
NC_001921.1	12,383	C	TTC	L	1118	F	13,097	C	GAC	L	1356	D
Bern stock*	12,383	C/G (50%)§	TTC/G	L	1118	F/L	13,097	C (100%)§	GAC	L	1356	D
AF378705.1	12,383	G	TTG	L	1118	L	13,097	C	GAC	L	1356	D
AF305419.1	13,100	G	TCG	L	1357	S	14,173	C	ACG	L	1715	T
NC_001921.1	13,100	T	TCT	L	1357	S	14,173	C	ACG	L	1715	T
Bern stock*	13,100	T (100%)§	TCT	L	1357	S	14,173	A (100%)§	AAG	L	1715	K
AF378705.1	13,100	A	TCA	L	1357	S	14,173	A	AAG	L	1715	K
AF305419.1	15,627	G	NA	NA (L 3′UTR)	NA	NA						
NC_001921.1	15,627	G	NA	NA (L 3′UTR)	NA	NA						
Bern stock*	15,627	A (100%)§	NA	NA (L 3′UTR)	NA	NA						
AF378705.1	15,627	A	NA	NA (L 3′UTR)	NA	NA						

Ref: GenBank accession number; gen pos: position of the nucleotide within the CDV genome; nt: nucleotide; ORF: open reading frame; aa pos: position of the amino acid within the protein sequence: aa: amino acid.
*Stock of CDV-OP in Bern (Switzerland).
NA: not applicable.
color-coded in red: the sequence comparison with the OP-CDV small plaque forming variant (AF378705.1) focused on the positions differing between the large plaque forming variants (AF305419.1 and NC_001921.1).
Red boxes: fixed (100%) amino acid differences between OP-CDV variants.
Light red boxes: non-fixed (<100%) amino acid differences between OP-CDV variants.
§ Percentage of reads exhibiting a mutation as compared to the reference sequence (AF305419.1).

(Fig. 1E and F; see below for more details concerning the minireplicon assay).

The mutation L-V13E was therefore introduced into the antigenomic cDNA clone (note that our pTM-L carried E13) and, indeed, both OP^{neon} and OP^{colorless} were very efficiently recovered. While green fluorescence confirmed the successful delivery of neon in OP^{neon}-infected cells, growth kinetics performed in Vero cells illustrated that only OP^{colorless} had similar profile as compared to OP stocks. In contrast, OP^{neon} displayed clear delayed growth kinetics (Fig. 1G). Hence, fusing neon to the N protein via the P2A motif did alter viral growth presumably because some residual uncleaved neon-P2A-N molecules may disturb viral replication. Collectively, these data validated the establishment of a robust OP-based reverse genetics platform.

When aligned with sequences of other members of the family *Paramyxoviridae*, it became obvious that the glutamate residue at position 13 of the L-protein was completely conserved. Interestingly, previous mutational works in the field were suggestive for a role of the N-terminal region of L in contributing to physical interaction with the P-protein (Bloyet et al., 2016; Cevik et al., 2004; Chattopadhyay and Shaila, 2004; Horikami et al., 1994; Malur et al., 2002). Furthermore, recent structural studies of the L/P complex of related viruses indeed highlighted multiple domains of L, including the N-terminal region, which were responsible for P-binding (Abdella et al., 2020; Gilman et al., 2019). We nevertheless attempted to more precisely decipher the mechanism underlying the negative impact of the L-V13 mutation on rescue efficiency. To this aim, indirect immunofluorescence (IF) analyses were initially performed to determine whether N, P and L co-localized in the cell. We employed epitope tagged version of N (FLAG)- and L (HA)-proteins to allow combinatorial IF analyses using anti-FLAG monoclonal antibody (mAb) (rabbit), anti-HA mAb (rat) and anti-P mAb (mouse) and subsequent treatment with fluorochrome-specific secondary antibodies. While single protein expression of P and HA-L (V13 and E13) revealed cytosolic staining, their co-expression did not exhibit any re-localization phenotypes, which precluded us to draw conclusions with regard to potential L/P interactions (not shown). Conversely, co-expression of FLAG-N and P led to clear accumulation of both proteins into cytoplasmic inclusion bodies, thereby validating their interactions (not shown). When co-expressed with FLAG-N and P, the HA-L-E13-protein was clearly redistributed to those inclusion bodies (Fig. 2A). Noteworthy, the HA-L-V13 exhibited very similar phenotypes as for HA-L-E13 (Fig. 2A). Taken together, these series of experiments indicated that substituting the charged residue at position 13 of L into a small hydrophobic amino acid did not modulate co-localization with the polymerase cofactor P-protein.

To focus our investigations more specifically on L/P protein-protein interactions, we conducted co-immunoprecipitation experiments (coIP). We first engineered truncated L-protein variants (aa 1–408; L^{trunc}). This strategy was employed because recently shown to increase MeV L solubility and thus facilitate coIP experiments (Bloyet et al., 2016). HA-L-^{trunc} (V13 and E13) were expressed in combination to P in BsrT7 cells, and upon cell lysis, P-proteins were pulled down using a mixture of three anti-P mAb (3568; 3698 and 4051 (Orvell et al., 1985)). Western blot analyses using anti-HA mAb revealed that the HA-L^{trunc}-V13E construct efficiently interacted with P. Although reduced, an association could also be recorded when HA-L^{trunc}-V13 was co-expressed with P (Fig. 2B). These data were consistent with the results recorded in IF experiments and further validated that the L^{trunc}-V13 variant did not lose physical interaction with the P-protein. Of note, omitting either the P- or L^{trunc}-expressing plasmids from the transfection mixture resulted in the absence of detectable HA-L^{trunc} bands, thereby confirming the specificity of the coIP assay. Altogether, and in agreement with recent structural studies (Abdella et al., 2020; Gilman et al., 2019), our data supported multiple domains of CDV L contributing to physical interaction with P.

We then determined the activity of both polymerase complexes (P+ L-V13 and P + L-V13E). We employed a newly generated OP-based bicistronic minireplicon (mRep), which was designed to express both the neon and Nano luciferase (nluc; Promega) reporter proteins (mRep-OP$^{neon/nluc}$; Fig. 3A). Strikingly, while concomitant delivery of the minigenome with N, P and HA-L-E13 in BsrT7 cells translated into high luminescence emission, switching HA-L-E13 with HA-L-V13 resulted in drastic impairments in polymerase activity. Indeed, luminescence values obtained with the HA-L-V13 variant barely exceeded those recorded when L was omitted from transfection mixtures (Fig. 3B). Collectively, although we cannot yet imply lack of efficient HA-L-V13/P interaction, impaired polymerase processivity or both phenotypes, as the molecular determinant(s) leading to the assembly of defective RdRp complexes, our results nevertheless unambiguously justified our inability to rescue OP^{neon} (harboring the L-V13 variation) from cDNA.

We further validated the efficiency of our newly established reverse genetics platform by rescuing a V protein-knockout recombinant virus (OP-V^{ko}; Fig. 1D). We conducted a combinatorial mutation approach to ablate V-expression. Indeed, such an approach may reduce the chances of *in vivo*-based reversion to virulence through recovery of wild-type (wt)-like V protein functions. Consistent with previous studies (Rothlisberger et al., 2010; Svitek et al., 2014; von Messling et al., 2006), removing the V-protein expression was initially performed by destroying the editing site (referred to as "kill edit"). To further mitigate possible recovery of the V-protein's functionalities, supplementary mutations were performed (i.e., potentially impacting diverse V functions, but without affecting the P-ORF). First of all, two additional stop codons (at positions R233 and K249) were introduced to ablate most of the V-specific C-terminal domain (reported to harbor essential functions in counteracting IFN production and action (Rothlisberger et al., 2010; Svitek et al., 2014)). Secondly, three substitutions were conducted at residues known to modulate productive interactions with: STAT2 (W246G and I247L) and MDA5 (E235A) (Svitek et al., 2014). Thirdly, the specific V motif (288-RVWH-291) demonstrated to potentially control PP1 phosphatases activity (and modulation of the MDA5 signal transduction) was also modified (288-GIGD-291) (Davis et al., 2014; Louber et al., 2015; Mesman et al., 2014). Finally, one mutation was introduced to disrupt the zinc-binding domain (ZBD; C255S) (Svitek et al., 2014).

Since we lacked anti-V antibodies cross-reacting with the OP V-protein, we investigated whether the RdRp polymerase complex of OP-V^{ko} was impaired at inserting an additional G nucleotide at the editing site (required to express V), as compared to the polymerase complex of

Table 3
Nucleotide changes associated with the insertion of the restriction sites.

Ref.	NruI	nt pos	NruI	nt pos	PmeI	nt pos	PmeI	nt pos	NotI	nt pos	NotI	nt pos
Bern stock	ACCAAT	102	ATATTC	1680	ATCCCTAA	1793	TCTGTAGC	3325	CCTAAAAA	3424	ATCATCAG	4440
Bern clone[#]	TCGCGA	102	TCGCGA	1680	GTTTAAAC	1793	GTTTAAAC	3325	GCGGCCGC	3424	GCGGCCGC	4440
Ref	MluI	nt pos	MluI	nt pos	RsrII	nt pos	RsrII	nt pos	BssHII	nt pos	BssHII	nt pos
Bern stock	AGCCCC	4929	AGTATT	6924	TCCAGCA	7072	AATCCCT	8894	TTAGCC	9024	CAGGTT	15,585
Bern clone	ACGCGT	4929	ACGCGT	6924	CGGACCG	7072	CGGACCG	8894	GCGCGC	9024	GCGCGC	15,585

Ref: Bern clone versus Bern stock; nt pos: position of the nucleotides (first underlined) within the CDV genome creating a restriction sites (Bern clone).
Color-coded in red: nucleotide substitutions (64 in total) performed to generate the indicated restriction site.

[#] cDNA clone (without reporters) constructed in this study derived from the reference sequence (AF305419.1) and harboring the L-V13E substitution as well as the mutations generating the unique restriction sites.

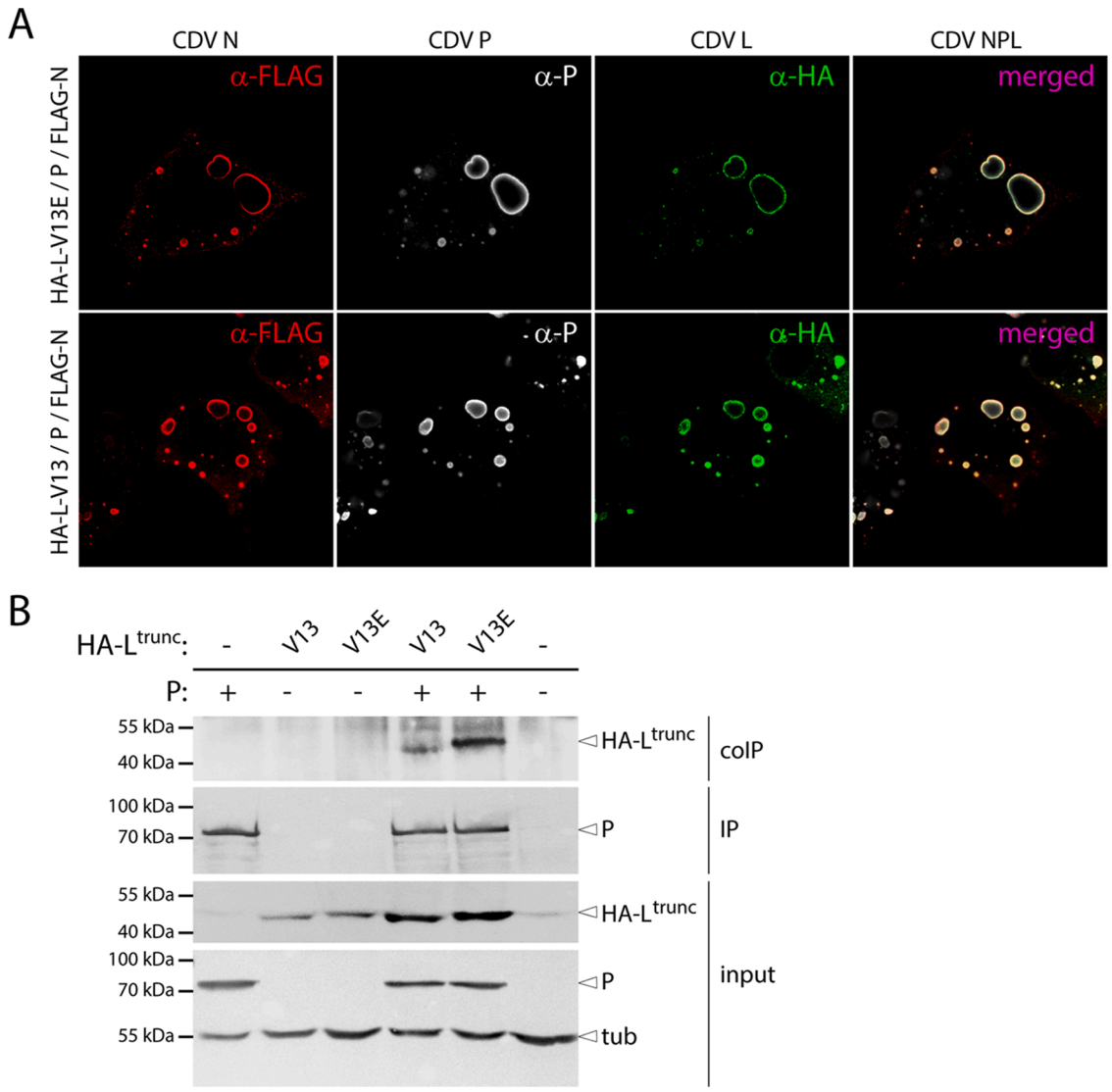

Fig. 2. Investigation of CDV P/L interactions. (A) Triple immunofluorescence (IF) analyses performed on Vero cells expressing FLAG-N (red)-, P (white)- and HA-L (green)-proteins. (B) Co-immunoprecipitation experiments of CDV P- and L-proteins. Total lysate of transfected cells is shown (input) as well as immune-precipitated P (IP) and co-immuno-precipitated L (coIP).

OP^{neon}. Upon total RNA extraction and cDNA production (from the mRNA population), a PCR fragment containing the standard (or mutated) editing site was amplified from the P-gene and subsequently cloned and sequenced. As expected, insertion of an additional G nucleotide (leading to the production of V) was exclusively observed in some clones obtained from OP^{neon}-infected cells, thereby strongly supporting the absence of V-protein expression by OP-V^{ko} (Fig. 1H). Next, using our minireplicon system (mRep-$OP^{neon/nluc}$), we confirmed identical polymerase activities regardless of whether the P-protein was expressed from the standard or mutated P-gene (Fig. 3C). We note that in this set of experiments, the C-protein was ablated from both P-expression vectors (pTM-P/C^{ko} and pTM-P/V^{ko}/C^{ko}). Interestingly, in Vero cells, growth kinetics of OP^{neon}-V^{ko} were delayed, although, 48 h post-infection, the virus eventually reached similar titers than OP^{neon} (Fig. 1G). Additionally, in presence type I IFN (1000 U/ml added two hour prior to infection), viral growth of V-expressing (including the original OP stock) and V-knockout viruses were strongly attenuated (Fig. 1I); a phenotype that was, at least in part, consistent with the fact that all viruses carried the Y110D mutation in the P-protein known to affect IFN-induced STAT1 nuclear translocation (Rothlisberger et al., 2010; Svitek et al., 2014).

While these data supported the notion that the OP V-protein could not significantly modulate the IFN-triggered antiviral state (V also carries the Y110D mutation within the N-terminal domain), they nevertheless illustrated that removing this component from infected cells led to recombinant viruses characterized by substantial growth kinetics impairments. We thus determined the impact of the OP V-protein on polymerase activity using our minireplicon system. We included the effect of OP M-, OP C- and GFP-proteins as controls (all cloned in the pTM vector). While GFP did not alter polymerase activity, a concentration-dependent inhibition was recorded with M. The impact of C was even more drastic, since already at the lowest concentration tested, inhibition of replication was substantial. In contrast, only the highest concentration of OP V exhibited the tendency to partially inhibit polymerase activity (~60%), although not to a significant manner (Fig. 3D). Interestingly, these findings are consistent with a reported MeV V-mutant (harboring two point mutations: Y113A/D114A), which also failed to potently restrict MeV replication (Witko et al., 2006). Overall, these data argued for a contributing role of a microdomain encompassing residues 110–114 of morbilliviral V-proteins in the regulation of replication.

In this study, we first report the establishment of an efficient rescue system based on an attenuated Onderstepoort (OP) CDV large plaque

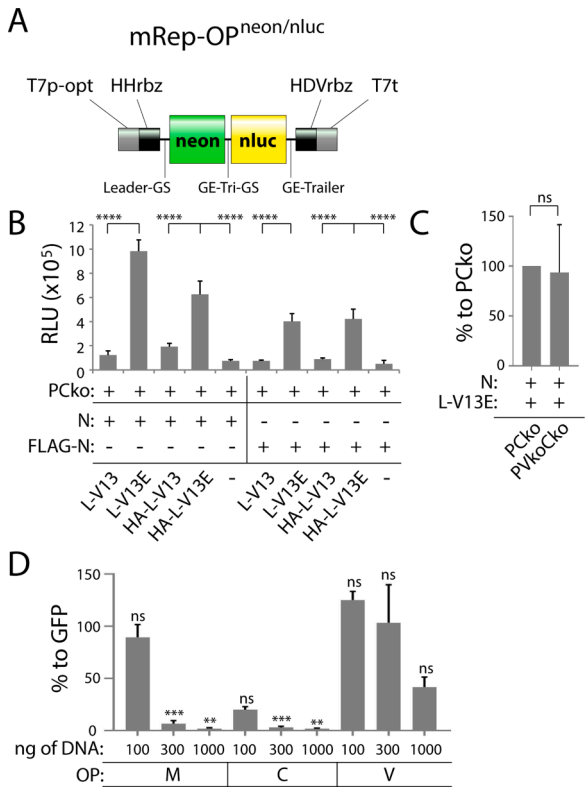

Fig. 3. Bioactivity of CDV polymerase complexes. (A) Illustration of the OP-based bi-cistronic minireplicon construct (mRep-OP$^{neon/nluc}$). Neon: mNeonGreen, nluc: Nano luciferase (Promega), T7p-opt: optimized T7 promotor sequence, HHrbz: hammerhead ribozyme sequence, HDVrbz: hepatitis D virus ribozyme sequence, T7t: T7 terminator sequence, GS: transcriptional gene start sequence, Tri: intergenic tri nucleotide sequence, GE: transcriptional gene end sequence. (B) Replication complex (P/L) activity. Luminescence emission was recorded 24 h post-transfection in BsrT7 cells. Means ± standard deviations of data from three independent experiments performed in duplicates are shown. (C) Replication complex activity of standard P protein and derivative version (harboring multiple silent mutations in the P-ORF). (D) Impact of OP-CDV M-, C-, V- and GFP-proteins on replication activity. The graphic shows means and SD for data from three independent experiments performed in triplicates. Significance was determined using one-way ANOVA using GraphPad Prism. ns, not significant *, $P < 0.05$; **, $P < 0.01$; ***, $P < 0.001$; ****, $P < 0.0001$.

forming variant. To achieve this, we have used a combination of modifications recently reported to significantly increase the robustness and efficiency of paramyxovirus rescue systems (Beaty et al., 2017). We then illustrated a strategy to engineer "green" recombinant CDV that did not rely on incrementing the number of viral transcripts; neon was coupled to N via the P2A peptide (neon-P2A-N). The derivative recombinant virus (OP^{neon}) exhibited impairments in growth kinetics compared to its "non-green" counterparts (OP stocks and OP^{colorless}). Interestingly, a similar P2A-based approach was recently demonstrated to have no major impact, including pathogenicity, when engineered on the matrix (M)-protein of a recombinant Nipah virus (a related paramyxovirus) (Park et al., 2016). This illustrates that varying impacts on viral replication depend on which protein is selected for P2A-engineering.

We also engineered a derivative V-knockout viral variant (through combinatorial mutations, which may strongly limit the chances of reversion to wild-type sequences) and demonstrated that the latter recombinant virus exhibited delayed replication kinetics *in vitro* than its V-expressing counterpart (even in IFN "production-defective" Vero cells); data that were in agreement with findings obtained with a virulent CDV strain (Svitek et al., 2014). Interestingly, the OP V-protein hardly restricted the viral polymerase complex activity; a phenotype that may be attributed to the Y110D substitution, which resides in a microdomain reported to affect MeV V ability to potently inhibit replication (Witko et al., 2006). Although additional studies are warranted to explain why CDV strains lacking V-expression exhibit growth kinetics impairments in Vero cells (and eventually in other cell types), all viruses investigated in this study (regardless of V-expression) were demonstrated to be strongly sensitive to IFN treatment. Interestingly, this phenotype may also corroborate with the fact that they harbored the Y110D mutation (present in both the P and V ORFs), which was reported to affect IFN-induced STAT1 nuclear translocation (Rothlisberger et al., 2010; Svitek et al., 2014). Collectively, these data were suggestive for a dual role of the wt V-protein 110–114 microdomain, *i.e.* control of replication efficiency and interference with innate immunity.

Finally, consistent with recent structural studies (Abdella et al., 2020; Gilman et al., 2019), we demonstrated that modifying a highly conserved glutamate residue locating at the N-terminal region of the L-protein by a hydrophobic amino acid was not sufficient to prevent the interaction with the polymerase cofactor P-protein. Rather, we demonstrated that the variant L-V13 displayed drastic defects in RdRp activity, which evidently precluded us to efficiently rescue OP from cDNA. These data highlighted the importance of residue L-E13 in contributing to the folding of productive polymerase complexes (P + L).

Using a similar cDNA clone (without the engineered restriction sites flanking the open reading frames), Gassen and colleagues rescued OP from a cDNA harboring L-V13 (AF305419.1), albeit very inefficiently compared to MeV (Gassen et al., 2000). While this seems contradictory to our findings (since our initial clone contained the L-V13 variation and was not rescued), it could be explained by the different procedures and cell lines used to rescue the recombinant virus. They described the L-E13V mutation only in the full-length cDNA clone and not in the L-expressing helper plasmid. Indeed, proper functionality of the latter was confirmed using minireplicon-based assay, thereby validating that this L-protein did not carry the defective mutation. Importantly, the authors employed the "vaccinia virus-dependent" system to express the T7 RNA polymerase necessary to initiate viral rescue (Gassen et al., 2000). Because replicating vaccinia virus catalyzes high-frequency of homologous recombination, we hypothesize that the full-length genomic cDNA clone could have been eventually repaired during some rescue attempts; an event that did not occur in our study because we employed the alternative "BsrT7-based" system for T7 RNA polymerase delivery. Alternatively, it is feasible that the single mutation L-V13E spontaneously emerged in some of their rescue attempts. Since this was one of the first morbilliviruses rescued, it was not standard practice to sequence the complete genome of the recombinant viruses, as is now possible with NGS technologies. Overall, (i) our inability to rescue a clone with a valine at position 13 of the L-protein, (ii) the demonstrated negative impact of L-V13 in a minigenome-based replication assay, and (iii) the fact that all investigated morbillivirus sequences carry the charged glutamate residue at this position of the polymerase (including another OP-CDV variant: NC_001921.1), suggests a potential sequencing issue with the deposited OP-CDV variant (AF305419.1), rather than the possibility to recover a viable recombinant virus harboring L-V13.

In summary, we developed a robust and highly versatile reverse genetics system based on a cDNA clone of a reported non-pathogenic strain of CDV (OP, large plaque-forming (Silin et al., 2007)), which required the recovery of the completely conserved glutamate residue at the N-terminal region of the L-protein. Noteworthy, the established system enabled us to implement a combinatorial mutation approach to ablate the expression of the V-protein, which may tackle with potential *in vivo* reversion to wild-type sequences. Such engineered viruses may additionally exhibit attractive profiles to generate next-generation multivalent vaccines with high potentials in veterinary medicine. Furthermore, OP^{neon} offers an ideal framework to provide novel insights into OP-CDV biology in general. Indeed, the discovery of putative new host cell entry factor(s) that promote(s) OP^{neon} infectivity in canine cancer cells may not only be of great interest to expand our knowledge

into a fundamental mechanism used by wild-type CDV to adapt its growth in cultured cells, but also to set the grounds to improve the oncolytic potential of the attenuated strain.

CRediT authorship contribution statement

Marianne Wyss: Conceptualization, Methodology, Data curation. **Vaiva Gradauskaite:** Conceptualization, Methodology, Data curation. **Nadine Ebert:** Visualization, Investigation, Methodology. **Volker Thiel:** Writing – review & editing. **Andreas Zurbriggen:** Writing – review & editing. **Philippe Plattet:** Conceptualization, Supervision, Funding acquisition, Investigation, Visualization, Writing – original draft, Project administration, Writing – review & editing.

Declaration of Competing Interest

The authors declare that they have no known competing financial interests or personal relationships that could have appeared to influence the work reported in this paper.

Acknowledgments

This work was supported by the University of Bern, the Swiss National Science Foundation (Ref. No. 310030_173185 to P.P. and SNSF CRSII5_183481 to R.R., P.P. and D.F.) and the OPO Foundation (to P.P.).

References

Abdella, R., Aggarwal, M., Okura, T., Lamb, R.A., He, Y., 2020. Structure of a paramyxovirus polymerase complex reveals a unique methyltransferase-CTD conformation. Proc. Natl. Acad. Sci. USA 117 (9), 4931–4941.

Beaty, S.M., Park, A., Won, S.T., Hong, P., Lyons, M., Vigant, F., Freiberg, A.N., tenOever, B.R., Duprex, W.P., Lee, B., 2017. Efficient and robust paramyxoviridae reverse genetics systems. mSphere 2 (2).

Bloyet, L.M., Welsch, J., Enchery, F., Mathieu, C., de Breyne, S., Horvat, B., Grigorov, B., Gerlier, D., 2016. HSP90 chaperoning in addition to phosphoprotein required for folding but not for supporting enzymatic activities of measles and Nipah virus L polymerases. J. Virol. 90 (15), 6642–6656.

Bodmer, B.S., Fiedler, A.H., Hanauer, J.R.H., Prufer, S., Muhlebach, M.D., 2018. Live-attenuated bivalent measles virus-derived vaccines targeting Middle East respiratory syndrome coronavirus induce robust and multifunctional T cell responses against both viruses in an appropriate mouse model. Virology 521, 99–107.

Buchholz, U.J., Finke, S., Conzelmann, K.K., 1999. Generation of bovine respiratory syncytial virus (BRSV) from cDNA: BRSV NS2 is not essential for virus replication in tissue culture, and the human RSV leader region acts as a functional BRSV genome promoter. J.Virol. 73 (1), 251–259.

Caignard, G., Bourai, M., Jacob, Y., Tangy, F., Vidalain, P.O., 2009. Inhibition of IFN-alpha/beta signaling by two discrete peptides within measles virus V protein that specifically bind STAT1 and STAT2. Virology 383 (1), 112–120.

Cattaneo, R., Russell, S.J., 2017. How to develop viruses into anticancer weapons. PLoS Pathog. 13 (3), e1006190.

Cevik, B., Holmes, D.E., Vrotsos, E., Feller, J.A., Smallwood, S., Moyer, S.A., 2004. The phosphoprotein (P) and L binding sites reside in the N-terminus of the L subunit of the measles virus RNA polymerase. Virology 327 (2), 297–306.

Chattopadhyay, A., Shaila, M.S., 2004. Rinderpest virus RNA polymerase subunits: mapping of mutual interacting domains on the large protein L and phosphoprotein p. Virus Genes 28 (2), 169–178.

Davis, M.E., Wang, M.K., Rennick, L.J., Full, F., Gableske, S., Mesman, A.W., Gringhuis, S.I., Geijtenbeek, T.B., Duprex, W.P., Gack, M.U., 2014. Antagonism of the phosphatase PP1 by the measles virus V protein is required for innate immune escape of MDA5. Cell Host Microbe 16 (1), 19–30.

de Vries, R.D., Ludlow, M., de Jong, A., Rennick, L.J., Verburgh, R.J., van Amerongen, G., van Riel, D., van Run, P., Herfst, S., Kuiken, T., Fouchier, R.A.M., Osterhaus, A., de Swart, R.L., Duprex, W.P., 2017. Delineating morbillivirus entry, dissemination and airborne transmission by studying *in vivo* competition of multicolor canine distemper viruses in ferrets. PLoS Pathog. 13 (5), e1006371.

Del Puerto, H.L., Martins, A.S., Milsted, A., Souza-Fagundes, E.M., Braz, G.F., Hissa, B., Andrade, L.O., Alves, F., Rajao, D.S., Leite, R.C., Vasconcelos, A.C., 2011. Canine distemper virus induces apoptosis in cervical tumor derived cell lines. Virol. J. 8, 334.

Devaux, P., Cattaneo, R., 2004. Measles virus phosphoprotein gene products: conformational flexibility of the P/V protein amino-terminal domain and C protein infectivity factor function. J.Virol. 78 (21), 11632–11640.

Duprex, W.P., McQuaid, S., Hangartner, L., Billeter, M.A., Rima, B.K., 1999. Observation of measles virus cell-to-cell spread in astrocytoma cells by using a green fluorescent protein-expressing recombinant virus. J.Virol. 73 (11), 9568–9575.

Fontana, J.M., Bankamp, B., Bellini, W.J., Rota, P.A., 2008. Regulation of interferon signaling by the C and V proteins from attenuated and wild-type strains of measles virus. Virology 374 (1), 71–81.

Frantz, P.N., Teeravechyan, S., Tangy, F., 2018. Measles-derived vaccines to prevent emerging viral diseases. Microbes Infect. 20 (9–10), 493–500.

Garcia, J.A., Ferreira, H.L., Vieira, F.V., Gameiro, R., Andrade, A.L., Eugenio, F.R., Flores, E.F., Cardoso, T.C., 2017. Tumour necrosis factor-alpha-induced protein 8 (TNFAIP8) expression associated with cell survival and death in cancer cell lines infected with canine distemper virus. Vet Comp. Oncol. 15 (2), 336–344.

Gassen, U., Collins, F.M., Duprex, W.P., Rima, B.K., 2000. Establishment of a rescue system for canine distemper virus. J. Virol. 74 (22), 10737–10744.

Gerke, C., Frantz, P.N., Ramsauer, K., Tangy, F., 2019. Measles-vectored vaccine approaches against viral infections: a focus on chikungunya. Expert Rev. Vaccines 18 (4), 393–403.

Gilman, M.S.A., Liu, C., Fung, A., Behera, I., Jordan, P., Rigaux, P., Ysebaert, N., Tcherniuk, S., Sourimant, J., Eleouet, J.F., Sutto-Ortiz, P., Decroly, E., Roymans, D., Jin, Z., McLellan, J.S., 2019. Structure of the respiratory syncytial virus polymerase complex. Cell 179 (1), 193–204 e114.

Horikami, S.M., Smallwood, S., Bankamp, B., Moyer, S.A., 1994. An amino-proximal domain of the L protein binds to the P protein in the measles virus RNA polymerase complex. Virology 205 (2), 540–545.

Hotard, A.L., Shaikh, F.Y., Lee, S., Yan, D., Teng, M.N., Plemper, R.K., Crowe, J.E., Moore, M.L., 2012. A stabilized respiratory syncytial virus reverse genetics system amenable to recombination-mediated mutagenesis. Virology 434 (1), 129–136.

Lamb, R.A., Parks, G.D., 2007. Paramyxoviridae: the viruses and their replication. Eds.. In: Fileds, B., Knipe, D.M., Howley, P.M. (Eds.), Paramyxoviridae: The Viruses and Their Replication. Fields' Virology, 5th ed. Lippincott Williams & Wilkins, Philadelphia, pp. 1449–1496.

Louber, J., Brunel, J., Uchikawa, E., Cusack, S., Gerlier, D., 2015. Kinetic discrimination of self/non-self RNA by the ATPase activity of RIG-I and MDA5. BMC Biol. 13, 54.

Maes, P., Amarasinghe, G.K., Ayllon, M.A., Basler, C.F., Bavari, S., Blasdell, K.R., Briese, T., Brown, P.A., Bukreyev, A., Balkema-Buschmann, A., Buchholz, U.J., Chandran, K., Crozier, I., de Swart, R.L., Dietzgen, R.G., Dolnik, O., Domier, L.L., Drexler, J.F., Durrwald, R., Dundon, W.G., Duprex, W.P., Dye, J.M., Easton, A.J., Fooks, A.R., Formenty, P.B.H., Fouchier, R.A.M., Freitas-Astua, J., Ghedin, E., Griffiths, A., Hewson, R., Horie, M., Hurwitz, J.L., Hyndman, T.H., Jiang, D., Kobinger, G.P., Kondo, H., Kurath, G., Kuzmin, I.V., Lamb, R.A., Lee, B., Leroy, E.M., Li, J., Marzano, S.L., Muhlberger, E., Netesov, S.V., Nowotny, N., Palacios, G., Palyi, B., Paweska, J.T., Payne, S.L., Rima, B.K., Rota, P., Rubbenstroth, D., Simmonds, P., Smither, S.J., Song, Q., Song, T., Spann, K., Stenglein, M.D., Stone, D. M., Takada, A., Tesh, R.B., Tomonaga, K., Tordo, N., Towner, J.S., van den Hoogen, B., Vasilakis, N., Wahl, V., Walker, P.J., Wang, D., Wang, L.F., Whitfield, A. E., Williams, J.V., Ye, G., Zerbini, F.M., Zhang, Y.Z., Kuhn, J.H., 2019. Taxonomy of the order Mononegavirales: second update 2018. Arch. Virol. 164 (4), 1233–1244.

Malur, A.G., Choudhary, S.K., De, B.P., Banerjee, A.K., 2002. Role of a highly conserved NH(2)-terminal domain of the human parainfluenza virus type 3 RNA polymerase. J. Virol. 76 (16), 8101–8109.

Mesman, A.W., Zijlstra-Willems, E.M., Kaptein, T.M., de Swart, R.L., Davis, M.E., Ludlow, M., Duprex, W.P., Gack, M.U., Gringhuis, S.I., Geijtenbeek, T.B., 2014. Measles virus suppresses RIG-I-like receptor activation in dendritic cells via DC-SIGN-mediated inhibition of PP1 phosphatases. Cell Host Microbe 16 (1), 31–42.

Muhlebach, M.D., 2017. Vaccine platform recombinant measles virus. Virus Genes 53 (5), 733–740.

Nakatsu, Y., Takeda, M., Ohno, S., Shirogane, Y., Iwasaki, M., Yanagi, Y., 2008. Measles virus circumvents the host interferon response by different actions of the C and V proteins. J.Virol. 82 (17), 8296–8306.

Nürnberger, C., Bodmer, B.S., Fiedler, A.H., Gabriel, G., Muhlebach, M.D., 2019. A measles virus-based vaccine candidate mediates protection against Zika Virus in an allogeneic mouse pregnancy model. J. Virol. 93 (3), :e01485–18.

Orvell, C., Sheshberadaran, H., Norrby, E., 1985. Preparation and characterization of monoclonal antibodies directed against four structural components of canine distemper virus. J.Gen.Virol. 66 (Pt 3), 443–456.

Park, A., Yun, T., Hill, T.E., Ikegami, T., Juelich, T.L., Smith, J.K., Zhang, L., Freiberg, A. N., Lee, B., 2016. Optimized P2A for reporter gene insertion into Nipah virus results in efficient ribosomal skipping and wild-type lethality. J. Gen. Virol. 97 (4), 839–843.

Parks, C.L., Wang, H.P., Kovacs, G.R., Vasilakis, N., Kowalski, J., Nowak, R.M., Lerch, R. A., Walpita, P., Sidhu, M.S., Udem, S.A., 2002. Expression of a foreign gene by recombinant canine distemper virus recovered from cloned DNAs. Virus Res. 83 (1–2), 131–147.

Patel, M.K., Goodson, J.L., Alexander Jr., J.P., Kretsinger, K., Sodha, S.V., Steulet, C., Gacic-Dobo, M., Rota, P.A., McFarland, J., Menning, L., Mulders, M.N., Crowcroft, N. S., 2020. Progress toward regional measles elimination - worldwide, 2000-2019. MMWR Morb. Mortal. Wkly Rep. 69 (45), 1700–1705.

Pfaller, C.K., Cattaneo, R., Schnell, M.J., 2015a. Reverse genetics of Mononegavirales: how they work, new vaccines, and new cancer therapeutics. Virology 479-480, 331–344.

Pfaller, C.K., Mastorakos, G.M., Matchett, W.E., Ma, X., Samuel, C.E., Cattaneo, R., 2015b. Measles virus defective interfering RNAs are generated frequently and early in the absence of c protein and can be destabilized by adenosine deaminase acting on RNA-1-like hypermutations. J. Virol. 89 (15), 7735–7747.

Pfaller, C.K., Radeke, M.J., Cattaneo, R., Samuel, C.E., 2014. Measles virus C protein impairs production of defective copyback double-stranded viral RNA and activation of protein kinase R. J. Virol. 88 (1), 456–468.

Pfankuche, V.M., Spitzbarth, I., Lapp, S., Ulrich, R., Deschl, U., Kalkuhl, A., Baumgartner, W., Puff, C., 2017. Reduced angiogenic gene expression in

morbillivirus-triggered oncolysis in a translational model for histiocytic sarcoma. J. Cell. Mol. Med. 21 (4), 816–830.
Plattet, P., Alves, L., Herren, M., Aguilar, H.C., 2016. Measles virus fusion protein: structure, function and inhibition. Viruses 8 (4), 112.
Plattet, P., Zweifel, C., Wiederkehr, C., Belloy, L., Cherpillod, P., Zurbriggen, A., Wittek, R., 2004. Recovery of a persistent Canine distemper virus expressing the enhanced green fluorescent protein from cloned cDNA. Virus Res. 101 (2), 147–153.
Ramachandran, A., Parisien, J.P., Horvath, C.M., 2008. STAT2 is a primary target for measles virus V protein-mediated alpha/beta interferon signaling inhibition. J.Virol. 82 (17), 8330–8338.
Robinson, S., Galanis, E., 2017. Potential and clinical translation of oncolytic measles viruses. Expert Opin. Biol. Ther. 17 (3), 353–363.
Röthlisberger, A., Wiener, D., Schweizer, M., Peterhans, E., Zurbriggen, A., Plattet, P., 2010. Two domains of the V protein of virulent canine distemper virus selectively inhibit STAT1 and STAT2 nuclear import. J.Virol. 84 (13), 6328–6343.
Shaffer, J.A., Bellini, W.J., Rota, P.A., 2003. The C protein of measles virus inhibits the type I interferon response. Virology 315 (2), 389–397.
Silin, D., Lyubomska, O., Ludlow, M., Duprex, W.P., Rima, B.K., 2007. Development of a challenge-protective vaccine concept by modification of the viral RNA-dependent RNA polymerase of canine distemper virus. J. Virol. 81 (24), 13649–13658.
Suter, S.E., Chein, M.B., von, M., V, Yip, B., Cattaneo, R., Vernau, W., Madewell, B.R., London, C.A., 2005. *In vitro* canine distemper virus infection of canine lymphoid cells: a prelude to oncolytic therapy for lymphoma. Clin.Cancer Res. 11 (4), 1579–1587.
Svitek, N., Gerhauser, I., Goncalves, C., Grabski, E., Doring, M., Kalinke, U., Anderson, D. E., Cattaneo, R., von Messling, V., 2014. Morbillivirus control of the interferon response: relevance of STAT2 and mda5 but not STAT1 for canine distemper virus virulence in ferrets. J. Virol. 88 (5), 2941–2950.
Tober, C., Seufert, M., Schneider, H., Billeter, M.A., Johnston, I.C., Niewiesk, S., ter Meulen, V., Schneider-Schaulies, S., 1998. Expression of measles virus V protein is associated with pathogenicity and control of viral RNA synthesis. J. Virol. 72 (10), 8124–8132.
Ungerechts, G., Engeland, C.E., Buchholz, C.J., Eberle, J., Fechner, H., Geletneky, K., Holm, P.S., Kreppel, F., Kuhnel, F., Lang, K.S., Leber, M.F., Marchini, A., Moehler, M., Muhlebach, M.D., Rommelaere, J., Springfeld, C., Lauer, U.M., Nettelbeck, D.M., 2017. Virotherapy research in Germany: from engineering to translation. Hum. Gene Ther. 28 (10), 800–819.
von Messling, V., Milosevic, D., Cattaneo, R., 2004. Tropism illuminated: lymphocyte-based pathways blazed by lethal morbillivirus through the host immune system. Proc. Natl. Acad. Sci. USA 101 (39), 14216–14221.
von Messling, V., Svitek, N., Cattaneo, R., 2006. Receptor (SLAM [CD150]) recognition and the V protein sustain swift lymphocyte-based invasion of mucosal tissue and lymphatic organs by a morbillivirus. J. Virol. 80 (12), 6084–6092.
von Messling, V., Zimmer, G., Herrler, G., Haas, L., Cattaneo, R., 2001. The hemagglutinin of canine distemper virus determines tropism and cytopathogenicity. J. Virol. 75 (14), 6418–6427.
Witko, S.E., Kotash, C., Sidhu, M.S., Udem, S.A., Parks, C.L., 2006. Inhibition of measles virus minireplicon-encoded reporter gene expression by V protein. Virology 348 (1), 107–119.
Yun, T., Park, A., Hill, T.E., Pernet, O., Beaty, S.M., Juelich, T.L., Smith, J.K., Zhang, L., Wang, Y.E., Vigant, F., Gao, J., Wu, P., Lee, B., Freiberg, A.N., 2015. Efficient reverse genetics reveals genetic determinants of budding and fusogenic differences between Nipah and Hendra viruses and enables real-time monitoring of viral spread in small animal models of henipavirus infection. J. Virol. 89 (2), 1242–1253.